Limnol. Oceanogr., 57(1), 2012, 000–000

doi:10.4319/lo.2011.57.1.0000

Three-dimensional simulation of lake and ice dynamics during winter

A. Oveisy,[a] L. Boegman,[a,*] and J. Imberger[b]

[a] Environmental Fluid Dynamics Laboratory, Department of Civil Engineering, Queen's University, Kingston, Ontario, Canada
[b] Centre for Water Research, University of Western Australia, Crawley, Western Australia, Australia

Abstract

An ice-formation algorithm is implemented in the three-dimensional Estuary and Lake Computer Model, to allow simulation of hydrodynamics and the thermal structure beneath the ice during winter. The one-dimensional governing equation of heat conduction among the three layers of white ice, blue ice, and snow is solved for the formation of ice cover considering the heat flux through air and water. This algorithm is applied independently in each grid cell within the simulation domain, allowing for spatially variable ice formation. The model was validated against observed data from both a large and a small Canadian mid-latitude lake (Lake Ontario and Harmon Lake, respectively). The lake surface temperature and the distribution and thickness of ice cover on Lake Ontario were predicted successfully during the 2006–2007 winter period. The model also accurately simulated spring 2007 temperature profiles, as typically used for the initial conditions for a summer simulation. The variation of ice and snow thickness, and vertical temperature profiles, were well-simulated for Harmon Lake during winter 1990–1991. These comparisons demonstrate the applicability of the model for year-round simulation of mid-latitude lakes of varying size.

Coupled hydrodynamic and biogeochemical computational lake models have been developed for simulation of lake circulation and management of water quality (Chapra 1997; Hodges 2009). However, attempts at simulation of water quality during winter have had mixed results and remain unpublished (*see* discussion in Gosink 1987). More recently, Hamilton et al. (2002) applied the one-dimensional (vertical) hydrodynamic and water quality model Dynamic Reservoir Simulation Model-Water Quality (DYRESM-WQ), coupled with an ice model to simulate the changes in tropic status in a small lake, resulting from atmospheric nutrient deposition and climate change. To our knowledge, simulation of lake biogeochemistry beneath ice cover in three dimensions has not been attempted. Consequently, processes such as winter primary production, the winter mixing of phosphorus (for example, which released from sediments during late-autumn hypoxia or introduced during the spring freshet) remain comparatively unexamined. Ice cover significantly modifies lake hydrodynamics, inhibiting wind stress, so that vertical mixing is sustained only by natural convection (Farmer 1975). Therefore, correct modeling of lake dynamics during the ice-covered season requires accurate simulation of ice cover and its effects on heat and momentum transfer.

Several thermodynamic models for ice formation have been developed over the past few decades. We find the existing models to be unsuitable for research on lake management, because they are either overly simplified three-dimensional (3D) ice-formation and transport models or more detailed one-dimensional (vertical) models that neglect water column dynamics and biogeochemistry. Most of these models are applying simplified assumptions for energy fluxes in the formation of ice (Maykut and Untersteiner 1971). Large-scale space–time simulation of ice formation coupled with dynamic atmospheric and ocean models was proposed by Parkinson and Washington (1979). Using 200-km resolution and four layers (atmosphere, snow, ice, ocean), they qualitatively simulated Arctic and Antarctic ice. More details of the ice-formation process were captured with the snow and ice version of DYRESM by Patterson and Hamblin (1988). Although this model (DYRESM-I) was one-dimensional (vertical), it incorporated a thermodynamic lake-mixing model of the water column beneath the ice and considered two-dimensional effects of partial ice cover. Gosink (1987) independently developed an ice-cover routine for DYRESM (DYRESM-ICE), which was successfully applied to Eklutna Lake, Alaska. These formulations of ice cover in DYRESM were suitable for high-latitude lakes, but lacked important processes necessary for mid-latitudes. The Mixed Lake with Ice (MLI) cover model of Rogers et al. (1995) extended the DYRESM-I model to include new process such as snowmelt due to rain, sediment heat transfer, formation of white ice, and variability of snow density and albedo, in order to address particular concerns at mid-latitudes. However, the underlying water-column dynamics were not considered in this study, because it was developed for shallow lakes with negligible thermal structure. In their model, the water temperature was predicted as function of the solar radiation reaching the water. McCord et al. (2000) developed the Dynamic Lake Model (DLM) for the study of artificial aeration kinetics in ice-covered lakes. The hydrodynamic component of DLM is very similar to DYRESM and the ice-cover sub-model is based on MLI.

Ice modeling in the Great Lakes began with Rumer et al. (1981), who simulated Lake Erie ice dynamics as a function of wind, currents, Coriolis force, and internal ice stresses, similar to Hibler's (1980), dynamic–thermodynamic sea-ice model, but with a more simple circulation model. They approximated the hydrodynamic transport of heat by lake currents by computing a steady-state current field using a vertically integrated equation of motion (Wake and Rumer 1979). Recently Yao et al. (2000) coupled the 3D Princeton

* Corresponding author: Leon.Boegman@civil.queensu.ca

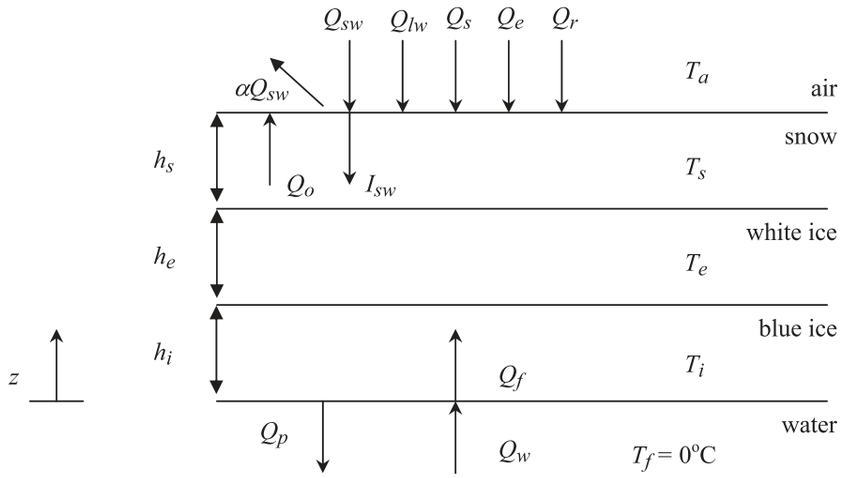

Fig. 1. Schematic showing the heat fluxes and vertical layers considered in the ice-cover model.

Ocean Model (POM) with the ice thermodynamics formulation of Hibler (1980), driven by monthly atmospheric forcing. Wang et al. (2010) used the similar approach of Yao et al. (2000) for simulation of ice and water circulation in Lake Erie for 2003–2004. These models coupled ice formation with POM, allowing for dynamic advection of ice. The approach to accretion and ablation of ice was simpler than that of Rogers et al. (1995), who simulated a single white-ice layer with no consideration of snow accumulation, and they assumed constant parameters for ice (i.e., ice albedo and conductivity) and neglected snowmelt due to rain, sediment heat transfer, and snow compaction, which are particularly important for mid-latitude lakes.

In the present study, an advanced ice-formation model, similar to that of Rogers et al. (1995), is coupled with the 3D hydrodynamic and biogeochemical Estuary and Lake Computer Model (ELCOM) with particular emphasis on simulation of mid-latitude lakes. The ice-formation algorithm is a quasi-steady solution of the heat transfer equation for three layers (blue ice, white ice, and snow) coupled to the lake-mixing model. The ELCOM solution grid is a Cartesian Arakawa C-grid and the governing equations are the Reynolds-averaged Navier–Stokes and scalar transport equations, with the assumption of hydrostatic pressure. A nonhydrostatic version of ELCOM is described in Botelho et al. (2009), and this may be used in small lakes when the focus is natural convection under ice and strong vertical velocities are induced. A turbulent-kinetic-energy–based mixed-layer model is used for vertical turbulent closure. The model uses a fixed, Z-coordinate finite difference mesh with Euler–Lagrangian approach for momentum advection. The free-surface evolution is calculated using vertical integration of the continuity equation in the water column. Details of ELCOM can be found in Hodges et al. (2000) and Hodges and Dallimore (2006). ELCOM has been applied extensively to study lake processes from the basin-scale (Hodges et al. 2000) to the large eddy scale (Botelho and Imberger 2007) and for biogeochemical and management studies when coupled with the Computational Aquatic Ecosystem Dynamics Model (Hillmer et al. 2008; Morillo et al. 2009). The implementation of an ice-cover routine increases the applicability of ELCOM, enabling both winter and multiyear lake-management studies in regions subject to ice cover. The model was validated against observed data from both a large and a small Canadian mid-latitude lake (Lake Ontario and Harmon Lake, respectively).

Ice model: Theoretical background

Following Rogers et al. (1995), we solve the steady-state equation for heat transfer among three contiguous layers of blue ice, white ice, and snow, between the atmosphere and water column, for each grid point at the surface of the lake. Figure 1 schematically demonstrates the heat fluxes and layers of snow and ice in the ice-formation algorithm. When the heat fluxes produce freezing temperatures (T_f) at the free-surface, ice starts to form. Imbalances in heat fluxes, between ice layers and the water column, result in changes in blue ice thickness. Snow accumulates on the blue ice surface; if the weight of snow exceeds the buoyancy of the ice, then white ice forms from flooded snow. More details of the ice-formation process are presented below. Because the solution is performed in all the nodes throughout the solution domain, spatial variation of the ice is expected. We do not model advective transport of ice.

In order to use the steady-state solution, we assume that the thermodynamic fluxes do not change significantly within a time step. Semtner (1976) showed that the assumption of quasi–steady state is accurate enough if the ice is thin. In other words, the temperature distribution reaches steady state within a time step. For the Gilpin et al. (1980) and Hill and Kucera (1983), showed that this assumption is valid when Stefan number (the ratio of sensible heat to latent heat) $S < 1$, where 3

$$S = \frac{C_i \Delta T}{L_w} \tag{1}$$

and L_w is latent heat of fusion of water, ΔT is the characteristic temperature difference, and C_i is the specific heat capacity of ice.

With the assumption of equilibrium heat fluxes in each time step, we can ignore the term for rate of heat change. In addition, because we neglect advection within the ice and snow cover, the steady-state heat conduction equation gives

$$\kappa_H \frac{\partial^2 T}{\partial z^2} = \frac{1}{\rho_n c_n} \frac{\partial Q}{\partial z} \tag{2}$$

where T is the temperature, Q is the heat flux, κ_H is the heat diffusivity, ρ_n is the snow or ice-cover density, c_n is the specific heat of snow or ice cover, and z is the vertical coordinate.

Defining the thermal conductivity $K = \kappa_h \rho_n c_n$, the penetrating radiation as

$$I = I_{sw} \exp[-\lambda(h-z)] \tag{3}$$

and considering the three distinct layers (i = blue ice, e = white ice, and s = snow) in Fig. 1, yields

$$\begin{aligned}
K_s \frac{\partial^2 T_s}{\partial z^2} &= A_1 \lambda_{s1} I_{sw} \exp[-\lambda_{s1}(h_i + h_e + h_s - z)] \\
&\quad + A_2 \lambda_{s2} I_{sw} \exp[-\lambda_{s2}(h_i + h_e + h_s - z)] + Q_{si} = 0, \\
&\quad h_i + h_e + h_s \geq z \geq h_i + h_e; \\
K_e \frac{\partial^2 T_e}{\partial z^2} &= A_1 \lambda_{e1} I_{sw} \exp[-\lambda_{s1} h_s - \lambda_{e1}(h_i + h_e - z)] \\
&\quad + A_2 \lambda_{e2} I_{sw} \exp[-\lambda_{s2} h_s - \lambda_{e2}(h_i + h_e - z)] = 0, \\
&\quad h_i + h_e \geq z \geq h_i; \\
K_i \frac{\partial^2 T_i}{\partial z^2} &= A_1 \lambda_{i1} I_{sw} \exp[-\lambda_{s1} h_s - \lambda_{e1} h_e - \lambda_{i1}(h_i - z)] \\
&\quad + A_2 \lambda_{i2} I_{sw} \exp[-\lambda_{s2} h_s - \lambda_{e2} h_e - \lambda_{i2}(h_i - z)] = 0, \\
&\quad h_i \geq z \geq 0;
\end{aligned} \tag{4}$$

where the incoming solar radiation I_{sw} ($I_{sw} = 1 - \alpha Q_{sw}$, where α is the albedo at ice and snow cover) has been divided into visible (subscript 1, $A_1 = 0.7$) and near infrared (subscript 2, $A_2 = 0.3$) according to Kirk (1983) and Boer (1980), and a distinct attenuation coefficient λ for each component and ice and snow layer. Q_{si} is the heat flux per volume released from white ice formation resulting from flooding of snow.

Temperature continuity and heat flux at interfaces of the layers are

$$\begin{aligned}
&T_i = T_f = 0 && z = 0 \\
&\left.\begin{aligned} T_i &= T_e \\ K_i \frac{\partial T_i}{\partial z} &= K_e \frac{\partial T_e}{\partial z} \end{aligned}\right\} && z = h_i \\
&\left.\begin{aligned} T_e &= T_s \\ K_s \frac{\partial T_s}{\partial z} &= K_i \frac{\partial T_i}{\partial z} \end{aligned}\right\} && z = h_i + h_e \\
&T_s = T_a && z = h_i + h_e + h_s,
\end{aligned} \tag{5}$$

where the indices f and a stand for freezing and air, respectively. Applying the boundary conditions in Eq. 5, the solution of Eq. 4 becomes

$$\begin{aligned}
&\left(\frac{h_s}{K_s} + \frac{h_e}{K_e} + \frac{h_i}{K_i}\right)(Q_o - I_{sw}) = (T_f - T_a) \\
&- I_{sw} A_1 \left[\frac{1 - \exp(-\lambda_{s1} h_s)}{K_s \lambda_{s1}} + \exp(-\lambda_{s1} h_s) \frac{1 - \exp(-\lambda_{e1} h_e)}{K_e \lambda_{e1}} \right. \\
&\quad \left. + \exp(-\lambda_{s1} h_s - \lambda_{e1} h_e) \frac{1 - \exp(-\lambda_{i1} h_i)}{K_i \lambda_{i1}} \right] \\
&- I_{sw} A_2 \left[\frac{1 - \exp(-\lambda_{s2} h_s)}{K_s \lambda_{s2}} + \exp(-\lambda_{s2} h_s) \frac{1 - \exp(-\lambda_{e2} h_e)}{K_e \lambda_{e2}} \right. \\
&\quad \left. + \exp(-\lambda_{s2} h_s - \lambda_{e2} h_e) \frac{1 - \exp(-\lambda_{i2} h_i)}{K_i \lambda_{i2}} \right] \\
&+ Q_{si} h_s \left(\frac{h_s}{K_s} + \frac{h_e}{K_e} + \frac{h_i}{K_i}\right) - \frac{Q_{si} h_s^2}{2 K_s}
\end{aligned} \tag{6}$$

With the value of heat flux at the air–ice or snow-cover interface (Eq. 7) and water and blue-ice interface (Eqs. 8, 9), Eq. 6 may be solved: 4

$$\begin{aligned}
&Q_o + Q_{lw} + Q_s + Q_e + Q_r = 0; \quad T_a < T_f = 0^\circ\mathrm{C} \\
&Q_o + Q_{lw} + Q_s + Q_e + Q_r = \rho_n L_w \frac{dh_n}{dt}; \quad T_a = T_f = 0^\circ\mathrm{C}
\end{aligned} \tag{7}$$

$$\begin{aligned}
Q_f = Q_o &- A_1 I_{sw} \{1 - \exp[-(\lambda_{s1} h_s + \lambda_{e1} h_e + \lambda_{i1} h_i)]\} \\
&- A_2 I_{sw} \{1 - \exp[-(\lambda_{s2} h_s + \lambda_{e2} h_e + \lambda_{i2} h_i)]\} - Q_{si} h_s
\end{aligned} \tag{8}$$

$$Q_w = -K_w \frac{dT_w}{dz} \tag{9}$$

where Q_0 is the incident solar radiation, Q_{lw} is the net longwave radiation, Q_s is the sensible heat flux, Q_e is the latent heat flux, and Q_r is the heat flux due to rainfall. Parameter t is time and L_w is the latent heat of fusion of water. Q_p is penetrative solar radiation, Q_f is the flux from ice to water, and Q_w is the flux from water to the ice. K_w is the water conductivity. Ice production and melting is the result of imbalance between Q_f and Q_w. 5

$$\frac{dh_i}{dt} = \frac{Q_f - Q_w}{\rho_i L_w} \tag{10}$$

Implementation in ELCOM

Equations 1–10 were implemented in the ELCOM surface-layer thermodynamics routine. To simulate the temperature and ice cover in the two Canadian lakes during winter, the following process descriptions, relevant to mid-latitude lakes, were applied.

Snow density—Snow can be flaky or watery, so its density can vary significantly. Snow can also be significantly compacted over time. We consider snow density variable due to compaction (Koren et al. 1999).

$$\rho_{s,c} = \rho_s \frac{\exp(Bw_s) - 1}{Bw_s} \tag{11}$$

where $\rho_{s,c}$ is the compacted snow density, w_s is the water equivalent in the snow, and B is calculated from

$$B = \Delta t C_1 \exp(0.08 T_s - C_2 \rho_s) \tag{12}$$

where $C_1 = 2.77 \times 10^{-4}$ m^{-1}s^{-1} and $C_2 = 0.021$ m^3 kg^{-1}. Unlike Rogers et al. (1995), who assumed constant density of the fallen snow as 80 kg m^{-3}, the fallen snow density is assumed to be a function of air temperature (Gottlieb 1980).

$$\rho_{s,new} = \max[50, 1.7(T_a + 15)^{1.5}] \tag{13}$$

and the average snow density was calculated from

$$\rho_s = \min\left(400, \frac{\rho_{s,c} w_{s,c} + \rho_{s,new} w_{s,new}}{w_{s,c} + w_{s,new}}\right) \tag{14}$$

where w refers to the relative water equivalent of the new fallen snow and the compacted snow, respectively.

Snow conductivity—Considerable increases in snow thermal conductivity may be expected when the snow density increases. The following equation (Ashton 1986) was used to describe the snow conductivity as the function of the snow density:

$$K_s = 0.021 + 4.2 \times 10^{-3} \rho_s + 2.2 \times 10^{-9} \rho_s \tag{15}$$

Snow and ice albedo—Ice and snow may show a wide range of albedo (Henderson-Sellers 1984), which mainly depends on the temperature of ice and snow and their thicknesses. Variation of ice and snow albedo is particularly important at mid-latitude lakes where rapid weather changes are expected; observation shows the albedo of ice and snow decreases with increasing temperature. The albedo of snow and ice (α_s), (α_i), respectively, were assumed variable in this study and calculated as follows (Vavrus et al. 1996):

$$\text{Ice:} \begin{cases} \alpha_i = 0.6 \rightarrow T_s \le -5^\circ\text{C} \\ \alpha_i = 0.44 - 0.032 T_s \rightarrow 0^\circ\text{C} \ge T_s \ge -5^\circ\text{C} \\ \alpha_i = 0.08 - 0.44 h_i^{0.28} \rightarrow \begin{matrix} h_i \le 0.5 \text{ m} \\ h_s \le 0.1 \text{ m} \end{matrix} \end{cases}; \tag{16}$$

$$\text{Snow:} \begin{cases} \alpha_s = 0.7 \rightarrow T_s \le -5^\circ\text{C} \\ \alpha_s = 0.50 - 0.04 T_s \rightarrow 0^\circ\text{C} \ge T_s \ge -5^\circ\text{C} \\ \alpha_s = \alpha_s(T_s) - \left(\frac{0.1 - h_i}{0.1}\right)[\alpha_s(T_s) - \alpha_i(T_i, h_i)] \rightarrow \begin{matrix} h_i \le 0.5 \text{ m} \\ h_s \le 0.1 \text{ m} \end{matrix} \end{cases} \tag{17}$$

Table 1. Parameters used in the ice and snow model (Rogers et al. 1995).

Parameter	Value
Ice visible solar attenuation coefficients (m^{-1})	6.00
Snow visible solar attenuation coefficients (m^{-1})	1.50
White-ice visible solar attenuation coefficients (m^{-1})	3.75
Ice infrared solar attenuation coefficients (m^{-1})	20.0
Snow infrared solar attenuation coefficients (m^{-1})	20.0
White-ice infrared solar attenuation coefficients (m^{-1})	20.0
Conductivity of blue ice (W m^{-1} °C^{-1})	2.00
Conductivity of white ice (W m^{-1} °C^{-1})	2.30
Specific heat of ice (kJ kg^{-1} °C^{-1})	2.10
Latent heat of fusion (kJ kg^{-1})	334
Blue-ice density (kg m^{-3})	917

White ice—When the ice is not able to support the weight of accumulated snow, the snow layer becomes flooded. The thickness of the flooded snow layer may be calculated by comparing the thickness of snow (h_s), to the maximum that can be supported by the existing blue ice ($h_{s,\max}$). A similar formulation as Rogers et al. (1995) was used to calculate the formation of white ice (thickness h_e) and heat released (Q_{si}):

$$h_{s,\max} = \frac{h_i(\rho_w - \rho_i) + h_e(\rho_w - \rho_e)}{\rho_s} \tag{18}$$

If $h_s > h_{s,\max}$, we calculate increase of white ice thickness and Q_{si}:

$$\Delta h_e = h_s - h_{s,\max}; \tag{19}$$

$$Q_{si} = \frac{(T_w c_a + L_f)\rho_w \frac{\Delta h_e}{h_s}\left(1 - \frac{\rho_s}{\rho_w}\right)}{\Delta t} \tag{20}$$

then set $h_s = h_{s,\max}$ and $h_e = h_e + \Delta h_e$.

Rain—In high-latitude lakes, it is rare to observe melting of snow by rain due to the very small chance of rain during the freezing season and also because of the sub-freezing temperature of snow (Parkinson and Washington 1979; Patterson and Hamblin 1988). However, in mid-latitude lakes it is not unusual to have frequent rain on top of previously fallen snow. The heat may increase the temperature and so result in melting. We calculate heat flux released from the rain to the snowpack by either sensible transfer or due to rain freezing as follows:

$$Q_r = \begin{cases} c_a \rho_o (T_a - T_s) R \rightarrow T_s = 0^\circ\text{C} \\ L_f \rho_o R \rightarrow T_s < 0^\circ\text{C} \end{cases} \tag{21}$$

where R is the amount and c_a the heat capacity of rain, respectively.

The model parameters used in this study are presented in Table 1.

Validation of the ice and snow model

The ice-formation model as described above was implemented in ELCOM and then validated against

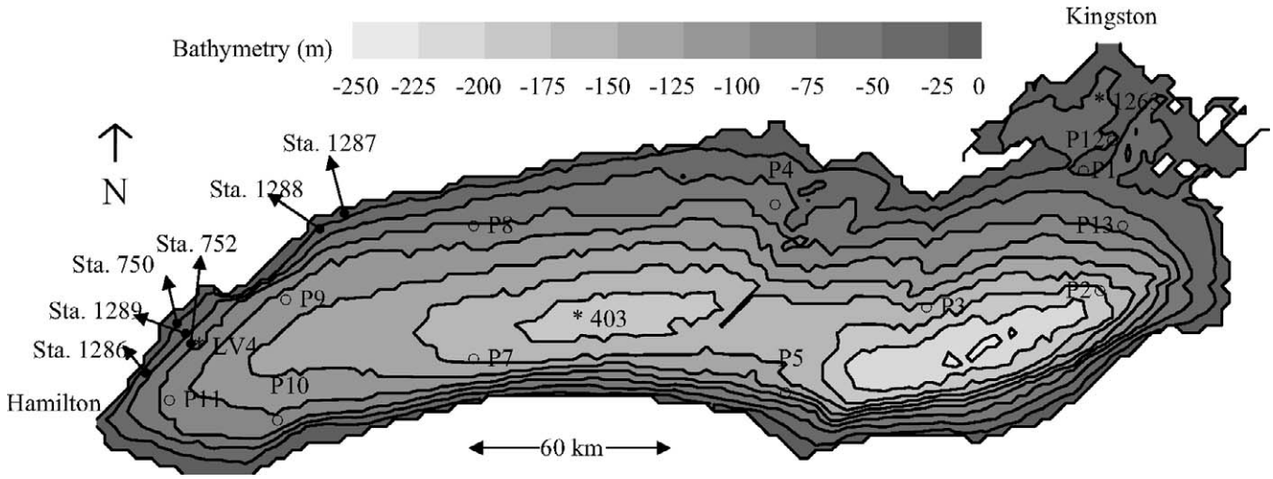

Fig. 2. Map of Lake Ontario bathymetry. Stations identified with an asterisk (IV4, 403, 586, and 1263) were used for the temperature profile initial condition. Stations identified with open circles were used for SST extraction points (Fig. 6). Filled circles show the locations of the Lake Ontario vertical temperature profile measurements that are compared with simulations results in Fig. 7.

observed data from a winter season in Lake Ontario (43.63 N, 77.92 W) and Harmon Lake (49.97 N, 120.70 W). These lakes were selected to test the performance of the model because they represent two extreme lake sizes and also have different space–time ice-cover characteristics.

Lake Ontario has approximate dimensions of 300 km × 120 km and a maximum depth of 250 m (Fig. 2).The maximum extent of lake ice is typically ~ 20% of the surface area, mostly at the shallow northeast end (Kingston Basin) where heat storage is minimal. Previous multiyear simulations of Lake Ontario, using an unstructured grid Finite Volume Coastal Ocean Model that neglected winter ice effects (Shore 2009), showed an ~ 2°C overestimation of spring water temperature (Wang et al. 2010).

Harmon Lake is a small sheltered lake in British Columbia, which is ~ 1200 m × 275 m with a maximum depth of 22 m (Fig. 3). The entire surface of Harmon Lake typically freezes during winter.

Following Wang et al. (2010), we quantify the capability of the model using the statistical measures of Mean Bias Deviation (MBD) and Root Mean Square Deviation (RMSD):

$$\mathrm{MBD} = 100\frac{\frac{1}{N}\sum_{i=1}^{N}(x_i - y_i)}{\frac{1}{N}\sum_{i=1}^{N} y_i}; \qquad (22)$$

$$\mathrm{RMSD} = \left[\frac{1}{N}\sum_{i=1}^{N}(x_i - y_i)^2\right]^{1/2} \qquad (23)$$

where x_i and y_i (i = 1,2,3,..N) are the model and observed variable time-series, respectively, and N is the total number of samples. MBD, which characterizes the bias of a model, is negative or positive if the model, respectively, under-predicts or over-predicts a variable. RMSD is the absolute error of the model against the observation.

Application to Lake Ontario

Model setup—The winter season of 2006–2007 was selected because ELCOM had already been used to accurately model the ice-free period (spring through autumn) of 2006 (Hall 2008; Boegman and Rao 2010). The model was initialized from rest on day 284 of 2006, with initial values taken from four in-lake measurement stations (Fig. 2) and interpolated throughout the domain using inverse distance methods, and was run until day 120 of 2007, a total of 201 d. The horizontal grid spacing was 2 km × 2 km and the model had 54 vertical layers, varying from 0.25 m near the surface to 16 m at the lake bed. Because Environment Canada moorings are removed from the lake during the ice-cover

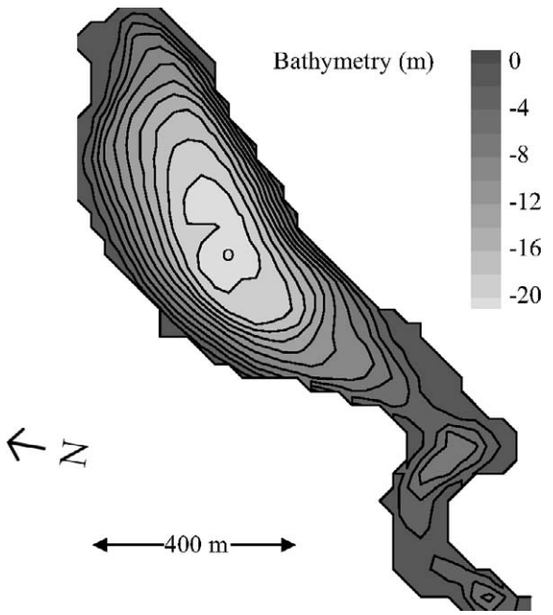

Fig. 3. Map of Harmon Lake bathymetry and location of measurement marked with an open circle.

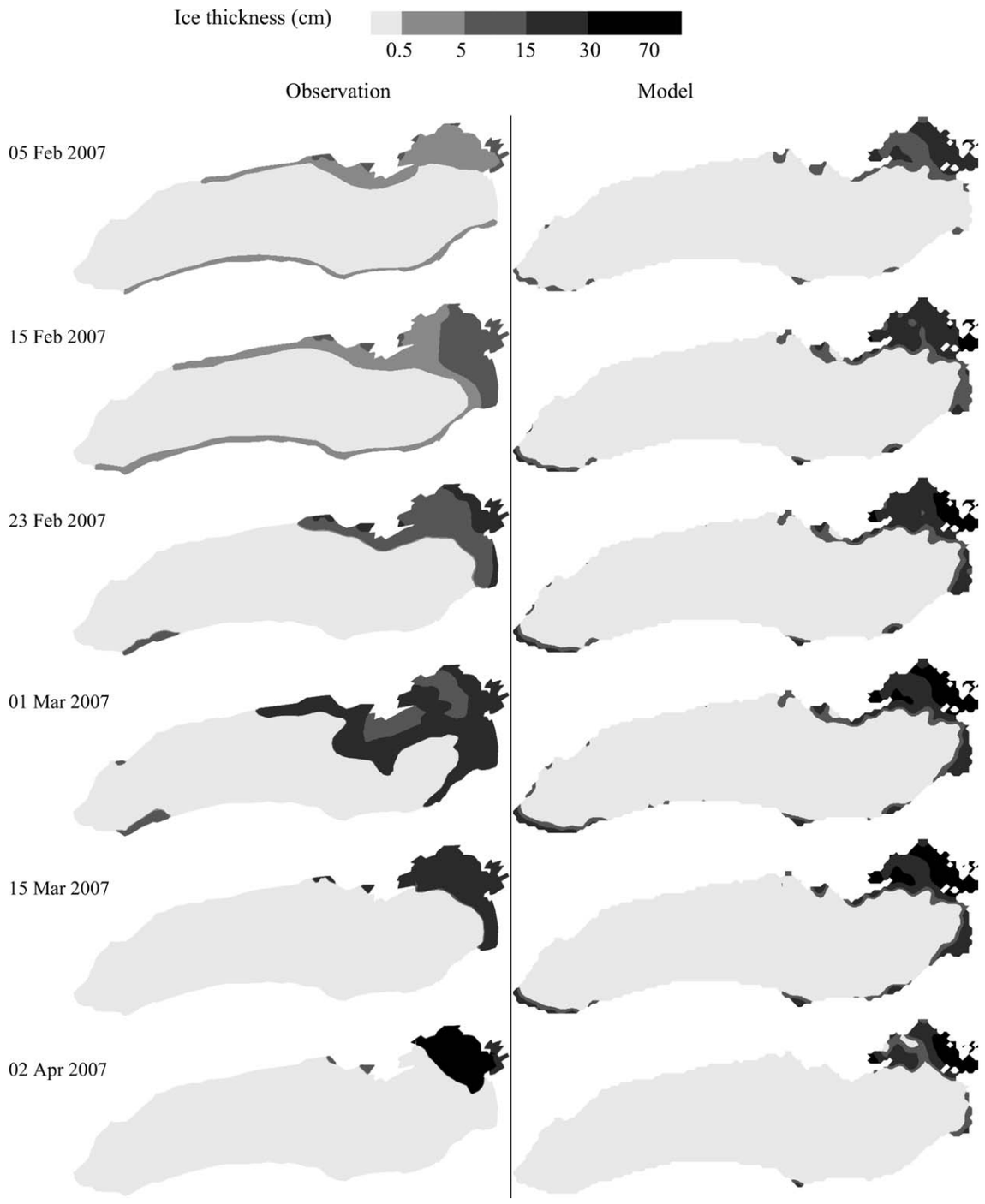

Fig. 4. Comparison of modeled and satellite-observed ice thickness on Lake Ontario during winter 2006–2007. Contour intervals were specified according to the satellite data.

season, for validation purposes the run period was chosen to overlap with the end of the 2006 measurement period and the beginning of the 2007 field season. The driving meteorological forces are from land stations at Hamilton (Burlington Pier, Environment Canada) and Kingston (Queen's University Integrated Learning Centre) and were interpolated onto 158 surface zones using an inverse distance method throughout the simulation domain. The wind velocities from land stations were first adjusted (mean and standard deviation) for the differences between over-land and over-lake conditions, through comparison of land data to over-lake data (Sta. 1263 and Sta. 403; Fig. 2).

During the ice-free portion of 2006 the input data for the simulation were wind velocity, air temperature, relative humidity, shortwave solar radiation, and lake-average precipitation. When the air temperature drops below freezing, the model interprets precipitation as snow with the associated density calculated by Eq. 13. The long-wave radiation was calculated in the model based on the difference between observed and clear-sky shortwave radiation.

We follow Patterson and Hamblin (1988) and define a minimum ice thickness of 0.1 m. Accurate determination of ice thicknesses near this limiting value remains a challenging problem in the current implementation. The ice dynamics at this limit are regulated by processes we do not model, including wind-induced turbulence, surface wave action, and underflow beneath the ice. Ice formed at thicknesses less than this value will be readily broken up by surface processes and advected. However, to account for broken ice, when the ice thickness is less than the minimum thickness, the model still uses the ice thickness in flux calculations.

Simulation results—The simulation results for ice thickness were compared against the Canadian Ice Services ice charts derived from satellite imagery (Nghiem and Leshkevich 2007). In general, the spatial pattern of ice formation and its temporal evolution is in favorable qualitative agreement with the observations (Fig. 4). There is greater spatial ice coverage in the observations during winter, but the observed ice is thinner than modeled. During spring, the observed and modeled ice has nearly identical spatial coverage and similar thicknesses. Errors in thickness may result from the model simulating both blue and white ice; whereas in the observations, these ice types are aggregated. Moreover, the satellite-derived ice-thickness observations presented in this study have not been ground-verified against direct ice-thickness measurements. Ice mostly forms in the northeast portion and marginally in the southwest of the lake, which is consistent with the observations. Lower water temperatures are associated with the smaller heat storage in the shallow-water depths in these regions and so favor ice formation. Persistent ice coverage also occurs in the shallow area along the north shore. In Fig. 5, the modeled ice coverage is reported as a percentage of the lake surface and it is within 5% of the observed value. In this figure, the volume of ice divided by the lake surface area is also presented, which is within 1.5 cm of the observation.

In addition to errors in ice observation, the discrepancies in Figs. 4 and 5 might be due to several other factors. In large lakes, ice drift is significant in the early periods of ice formation and the lack of advective ice dynamics in the ice-formation model could lead to errors in simulation because ice could be transported by wind and hydrodynamic forces. For example, comparison of the ice charts on 15 March and 02 April shows increases in the ice thickness near shore, while the ice is disappearing in deeper parts of the lake. The reasons for this process may be due to ice transport by the wind toward nearshore areas. The other factor that contributes to the discrepancies may be the rather large 2-km horizontal grid in resolving bathymetry in nearshore regions—in particular, near the Kingston Basin where there are numerous islands and lakebed channels.

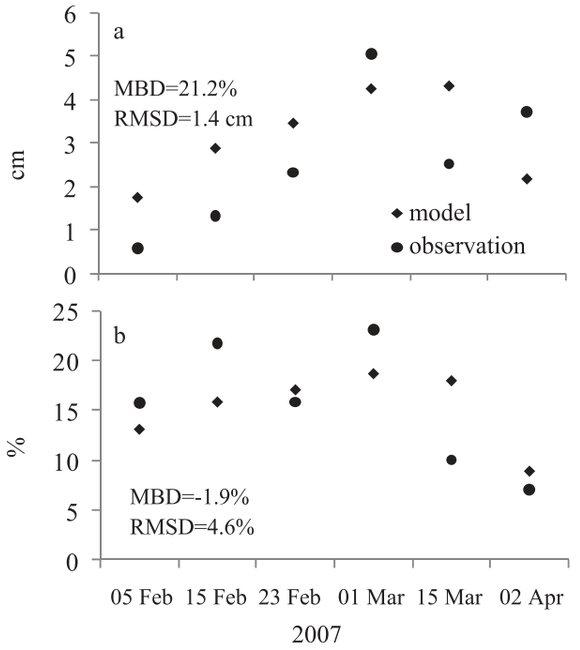

Fig. 5. Quantitative comparison of modeled and observed ice distributions. (a) Total volume of ice divided by the surface area of the lake in (cm), and (b) percentage of the lake surface covered with ice.

Ideally, such a large domain needs to be forced using spatially accurate metrological data. Inclusion of data from a third land station at Oswego, New York resulted in the pattern of ice formation being significantly different from observations and increased ice coverage in the south and southeast of the lake. This undesirable pattern could be due to the quality of data at this station, or the relevancy of the data for over-lake metrological forcing. Therefore, special care has to be taken in choosing and correcting metrological data, and the model must be validated against observations to ensure deficiencies in winter meteorological forcing are not leading to erroneous results.

Better estimation of the model parameters for a specific lake could result in better ice-thickness prediction, because the results were highly sensitive to the input parameters. For example, the albedo of snow significantly changes, from 0.95 for freshly fallen snow to 0.2 for slushy, gray, melting snow (Henderson-Sellers 1984). Choosing the wrong value can significantly affect the heat reception of the lake. The modeled lake temperatures were validated against satellite-derived sea surface temperatures (SST) at 11 locations (Fig. 2) in the lake during the winter of 2006–2007 (Fig. 6). In-situ mooring data were not available during this period because moorings are removed during the winter ice season. The observation temperature is based on satellite imagery and was provided by Great Lakes Environmental Research Laboratory of National Oceanic and Atmospheric Administration; the modeling results follow the observation with few discrepancies, the average MBD and RMSD for all the locations shown are -2.5% and 1.0°C, respectively, showing that the model slightly under-predicts the SST. Cyclic variation of air temperature, resulting from atmospheric storm-front activity

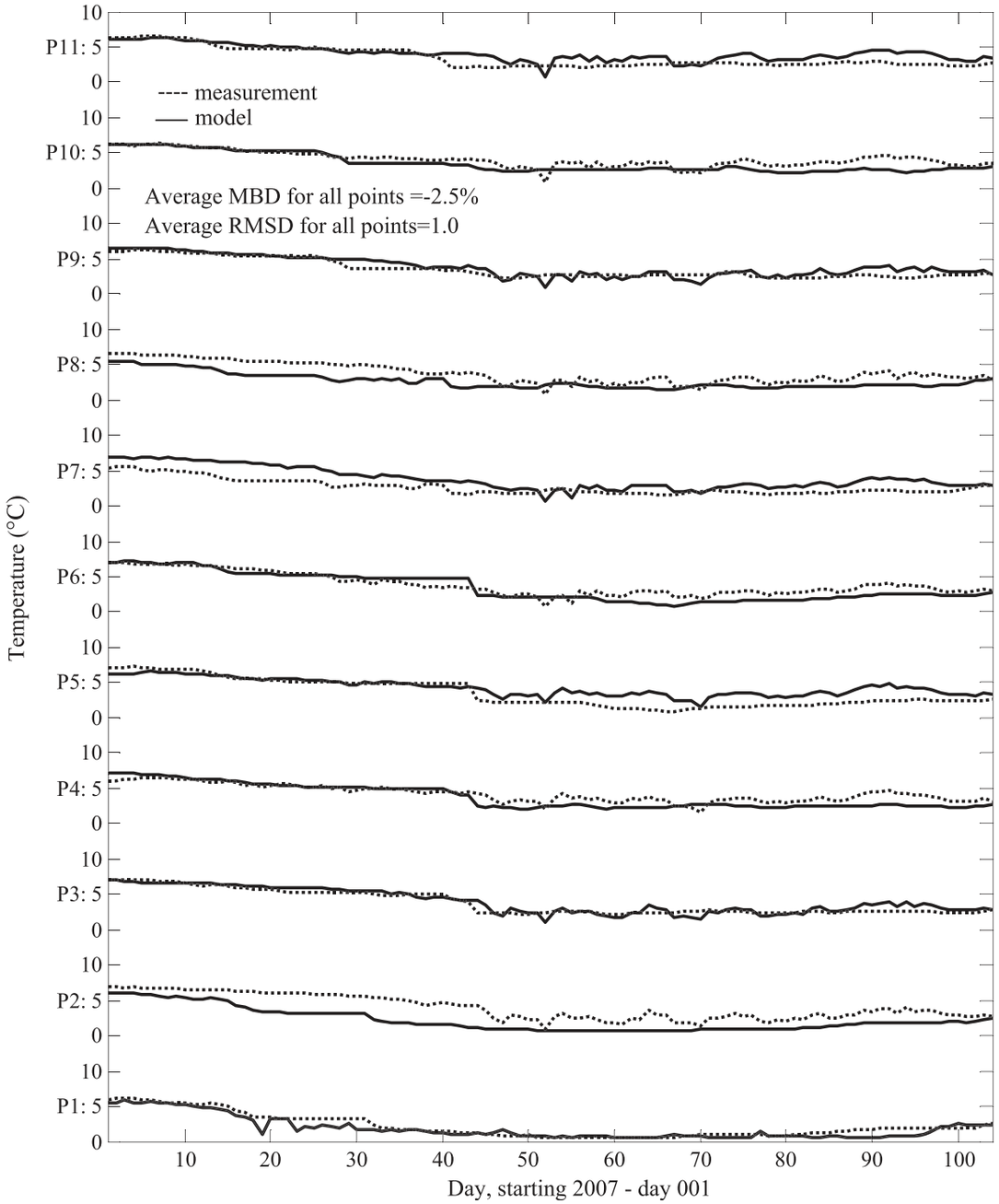

Fig. 6. Comparison of modeled and observed sea surface temperature (SST). Observations are derived from satellite observations. Locations of comparisons are indicated on Fig. 2.

with a 10-d period (Hamblin 1987) can be seen in the observed and simulated SST. At point P1 in Fig. 2, for the majority of time the SST is close to zero because it is under ice cover; the temperature increases in spring when the ice cover melts.

ELCOM also reproduced the vertical profiles of water temperature at six stations (Fig. 2) on day 106 of 2007. The model shows agreement with the temperature profiles at all stations with $< 1^{\circ}C$ difference (Fig. 7). The model error will be partially a result of the coarse 2-km gridding not resolving nearshore temperature patchiness and small-scale topographic features. The water column was below the temperature of maximum density of $4^{\circ}C$, causing both modeled and observed profiles to exhibit reverse winter stratification, with temperatures decreasing toward the surface.

Modeled contours of temperature profiles at P12 and P13 (Fig. 2) show the differences in water-column dynamics occurring as a function of depth (Fig. 8). The relatively shallow water column ($\sim$ 25-m depth) at P12 cooled much faster than the deeper water ($\sim$ 50-m depth) at P13, after the autumn turnover; P12 then experienced a significant

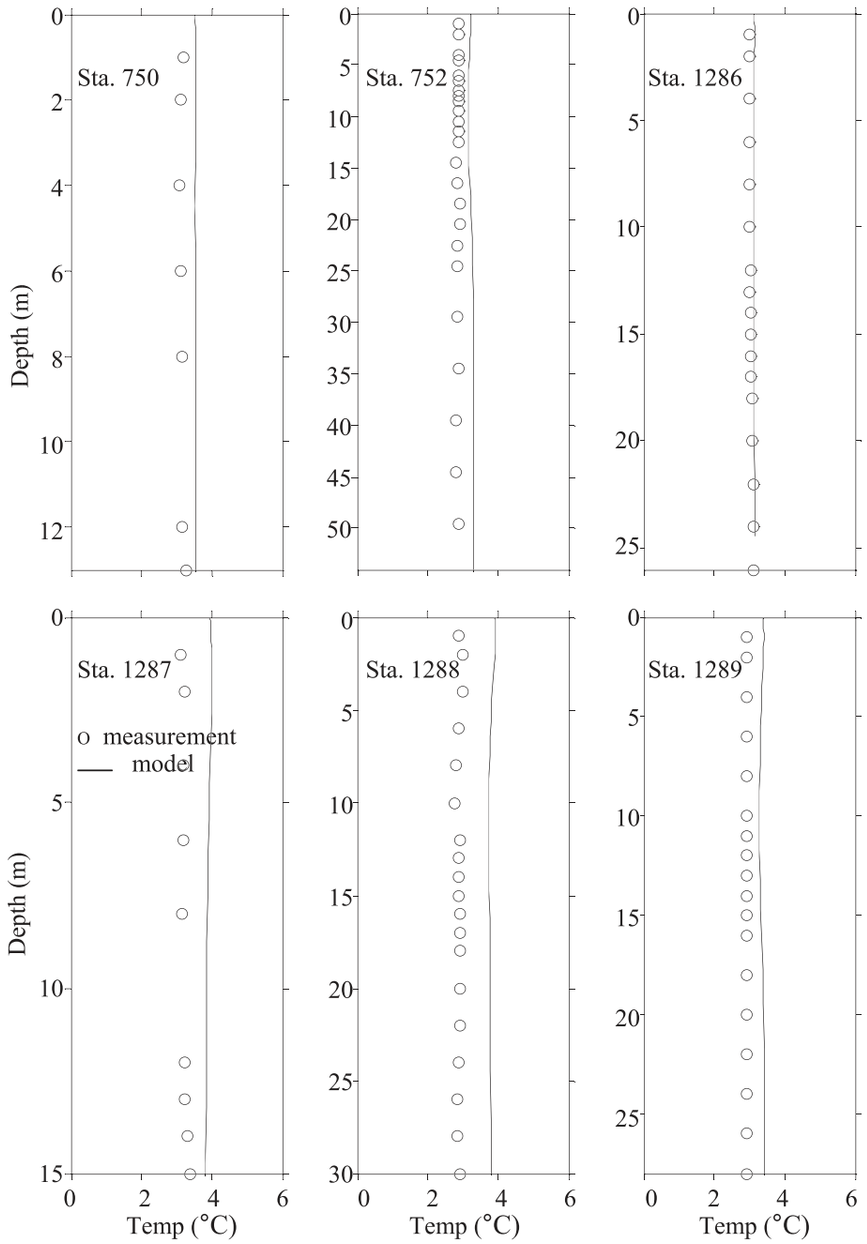

Fig. 7. Vertical profiles of temperature (Temp) on day 106 of 2007 at time 00:00 h. The locations of the profiles are shown in Fig. 2. The measurements were taken using Tidbit loggers that have an accuracy of ± 0.2°C.

period of ice cover and zero surface temperatures. The strong sheltering effect of the ice is seen clearly by observing the modeled rate of dissipation of turbulent kinetic energy for this period, at P13 relative to P12, where no ice cover was predicted by the model and temperatures remained above freezing (Fig. 9). At P13, dissipation was reduced where the water column remains weakly stratified. At both stations the reverse winter stratification, spring turnover, and onset of seasonal stratification are clearly recognizable. These comparisons confirm that good predictions of both the surface and the vertical temperature conditions may be achieved from autumn to the start of the spring season. Because ELCOM has been shown to model accurately the Lake Ontario thermal structure and hydrodynamics from spring turnover through autumn turnover during 2006 (Hall 2008; Boegman and Rao 2010), the model is now capable of year-round simulation.

Application to Harmon Lake

Model setup—The winter season from the 13 December 1991 to 24 March 1992 was chosen to model Harmon Lake

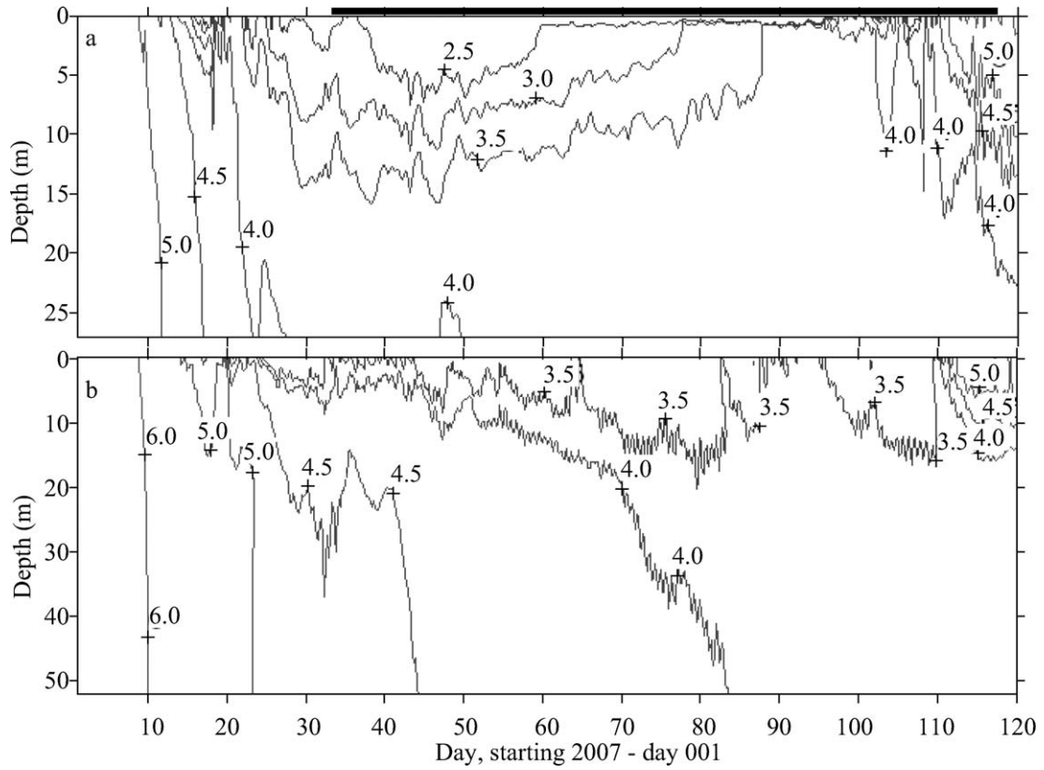

Fig. 8. Contours of modeled temperature time-series (°C) under (a) ice-covered, and (b) ice-free stations in the Kingston Basin of Lake Ontario. Sta. (a) P12, and (b) P13 are indicated on Fig. 2. Note the different vertical scales. The black line above panel denotes the period of ice cover.

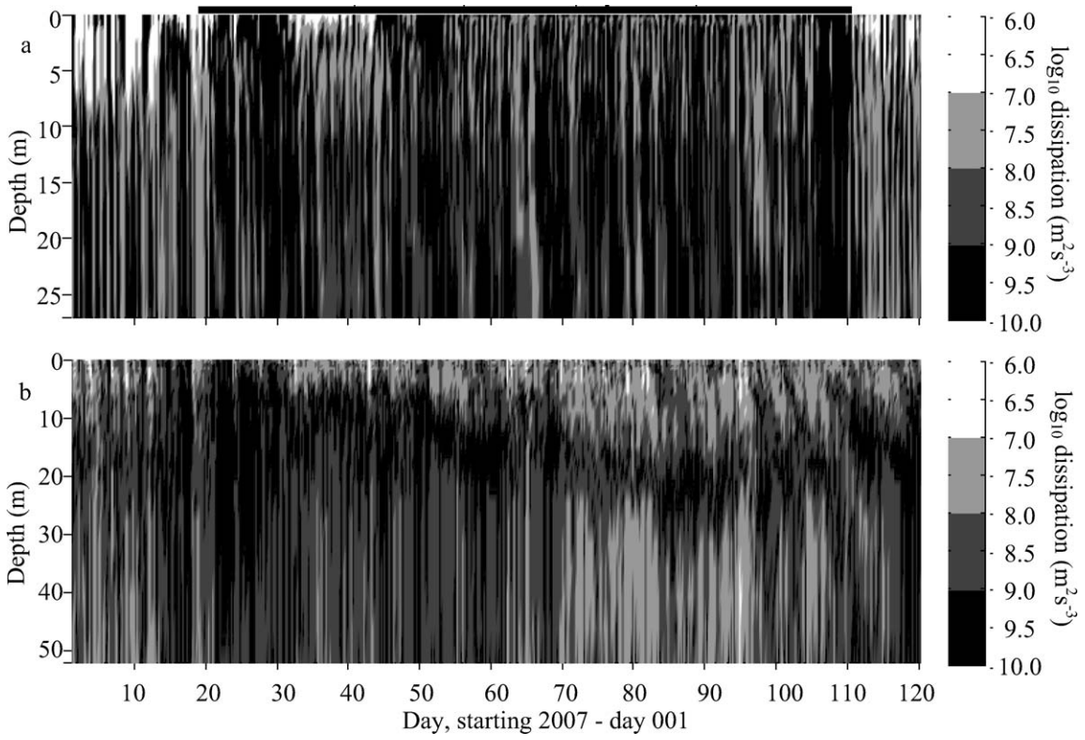

Fig. 9. Depth vs. time contours of modeled dissipation of turbulent kinetic energy ($\log_{10}$ dissipation) in Lake Ontario at Sta. (a) P12, and (b) P13. Note the different vertical scales. The black line above panel indicates the period of ice cover.

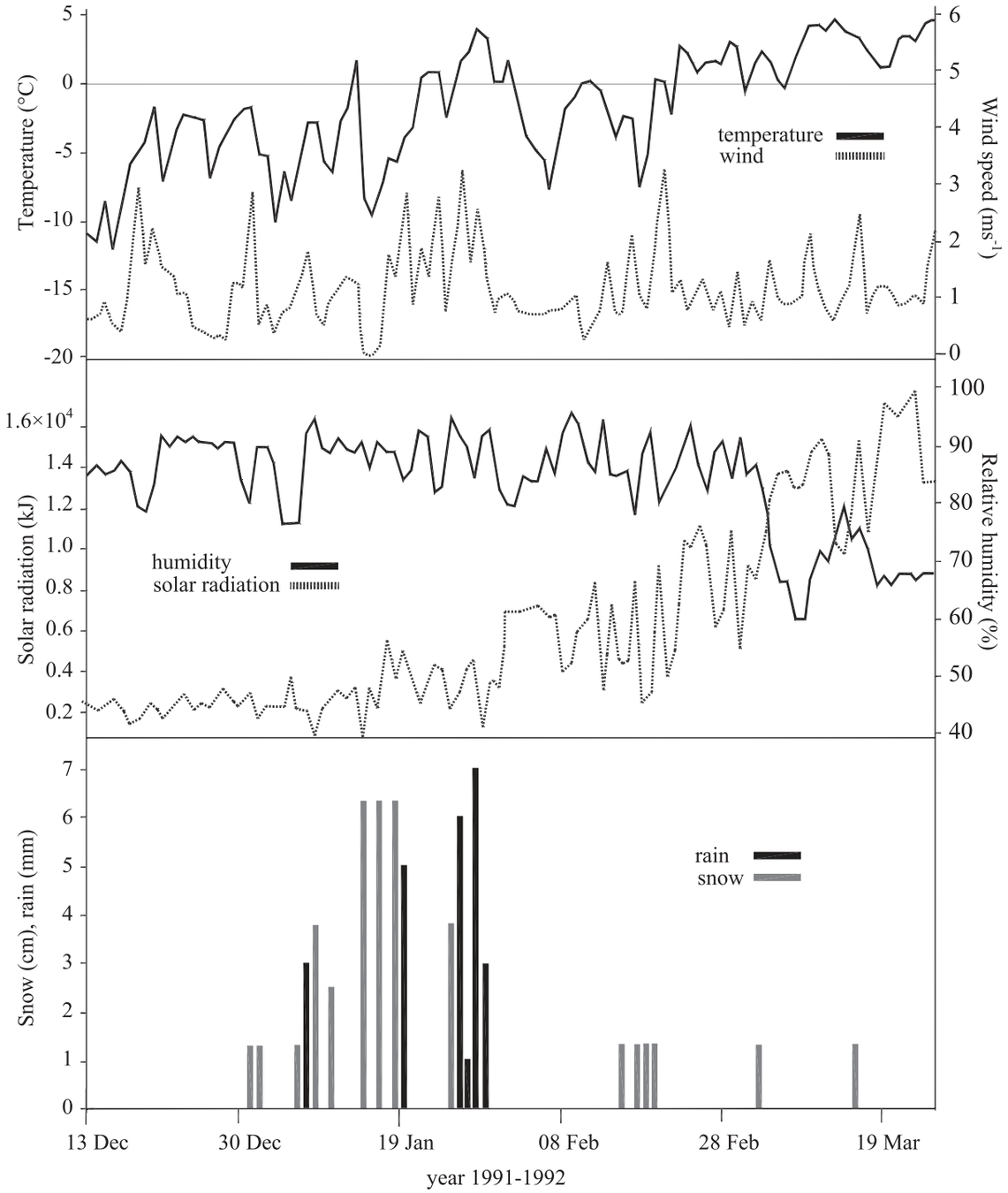

Fig. 10. Meteorological data collected at Menzies Lake, 13 December 1991–27 March 1992. Rain values are from Merritt, which is located 15 km northwest of Harmon Lake. Data have been digitally reconstructed from Rogers et al. (1995).

because data were available for this period (Rogers et al. 1995): in general, there exist very little data (e.g., ground-measured ice and snow thickness and lake temperature) from ice-covered lakes (Bengtsson 1996).

A 50-m × 50-m horizontal grid was applied with 53 vertical layers, ranging from 0.25 m at the surface to 0.5 m near the bed. Meteorological data (including solar radiation, wind speed, relative humidity, and air temperature [Fig. 10] for this simulation), as reported in Rogers et al. (1995), were measured at Menzies Lake, about 5 km northeast of Harmon Lake and 100 m higher in elevation. Rainfall was measured at Merritt, 15 km northwest of Harmon Lake, and snowfall was measured using snow-board observations (accuracy $> \pm 1$ cm) after each snow event. Wind direction was not reported in Rogers et al. (1995), because their 1D vertical model does not require

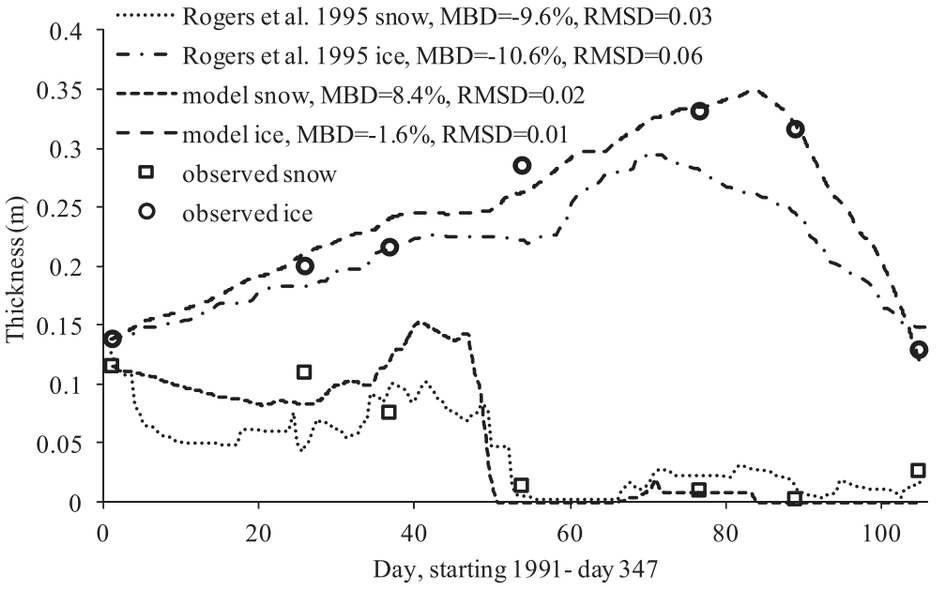

Fig. 11. Comparison of modeled and observed ice and snow thicknesses at Harmon Lake during 1991–1992. Modeled time-series are daily output from the present study and results from the MLI model (Rogers et al. 1995). The less frequent observations are described fully in the text.

this input. We used wind direction from metrological station at Merritt. In the specific case of modeling Harmon Lake, the lake was ice covered during whole simulation and wind had no drag forces on the water surface; therefore, direction of wind does not have any significant effect on the outcome of the model.

Ice and snow thickness (there was no distinction between blue ice and white ice) were measured during several field trips to Harmon Lake at the deepest part of the lake (Fig. 3). Vertical profiles of water temperature were also measured at the same location. Because much compaction can take place over the first 24 h following a snowfall, and because the snow boards may not have been ideally placed with respect to exposure, the errors in estimating the actual depth of snowfall are probably much greater (Rogers 1992). Because of potential inaccuracies in precipitation measurements, relative to local conditions and the strong influence of precipitation on ice formation, the observed snow and rainfall values (Fig. 10) were compared with the snow-thickness observations at Harmon Lake (Fig. 10) in order to make any necessary adjustments. The snowfalls were found to be much higher than the increase in snow depth; for example, from 15 January to 19 January about 19 cm of snow was measured and during this period the air temperature was significantly below freezing, but snow thickness on 19 January was about 7 cm and was actually less than the depth of snow on 14 January. Although significant snow compaction was not expected for this period, snow transport could be one of the reasons for these differences (Rogers et al. 1995). For adjustment, using observed snow depths, we assumed one-third of the observed snowfall at Menzies Lake for modeling of Harmon Lake. In addition, the precipitation was adjusted based on air temperature: when the air temperature was above or below the freezing point, the precipitation was converted to rain or snow, respectively. The model was initialized on 13 December 1991, with observed initial conditions of snow and ice thicknesses of 14 cm and 12 cm, respectively (Fig. 11). There was assumed to be no white snow as an initial condition, because the initial ice thickness could tolerate the initial weight of the snow on top of it. The initial condition for water temperature was the measured vertical profile of temperature on 13 December (Fig. 12). Rates of sediment heat transfer at both mid- and high-latitude lakes during ice-covered periods are typically in the range of 1–5 Wm^{-2} (Birge et al. 1927; Likens and Johnson 1969; Ashton 1986), considering sediment heat fluxes can contribute to internal mixing, particularly in small lakes (Mortimer and Mackereth 1958; Welch and Bergmann 1985). In this simulation, 1 Wm^{-2} is assumed for heat release from sediment to the lake. We assumed 0.02 for the albedo of ice (Rogers et al. 1995).

Simulation results—As seen in Fig. 11 for the first 80 d, the ice thickness increased from $\sim$ 0.15 m to 0.35 m over, the simulations closely following the observations. The increase in thickness resulted from below-freezing air temperatures and low-incident shortwave radiation characteristic of winter conditions (Fig. 10). The initial snow thickness on top of the ice first decreased due to compaction (to day 23), then increased with increasing snowfall (day 25 to day 38), but this melted to a near-zero thickness, due to significant rainfall (Fig. 11, day 50; Fig. 10, 20 Jan). Coupling between ice and snow is illustrated by the model results; the heavy snow (Fig. 11, days 30–40; Fig. 10, 30 Dec–19 Jan) acted to insulate the ice and slowly increased in ice thickness during this time. The ability of the model to capture these rapid responses of snow and ice dynamics to daily changes in meteorological conditions emphasizes the importance of implementing

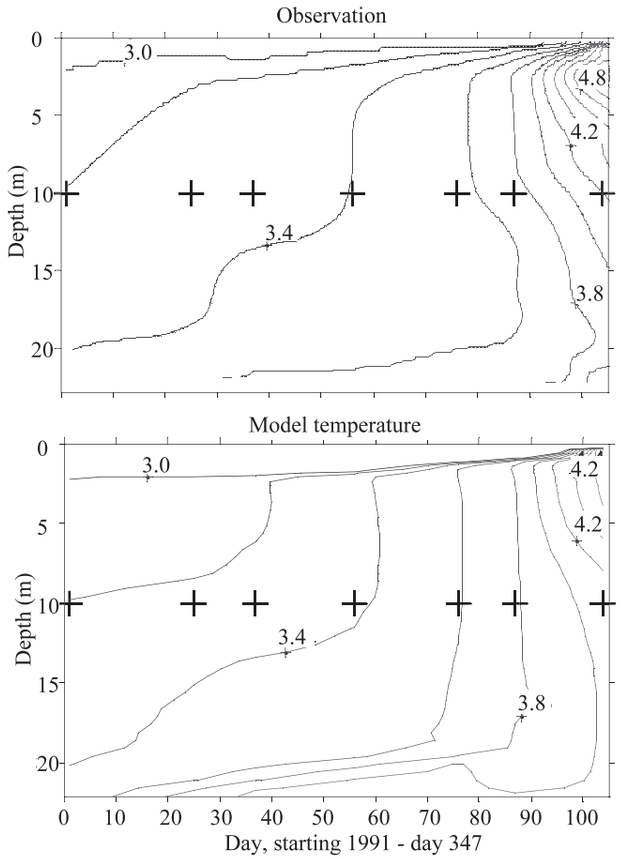

Fig. 12. Contours of modeled and observed water-column temperature in depth vs. time space for Harmon Lake. Isotherms have been computed by linearly interpolating model output at discrete depths. The observed data were digitally reconstructed from Rogers et al. (1995), and the crosses indicate the days when vertical profiles of temperature were measured. The isotherms below 3°C are not shown on the figure for clarity of presentation. The entire period shown is ice-covered.

snow- and ice-melting due to rain in the ice algorithm. Toward the end of the simulation, the air temperatures increased above freezing and solar radiation also increased (Fig. 10) leading to a decrease in ice thickness. In Fig. 11, the MLI modeling result is also presented. The main reasons for the better performance of ELCOM, compared to MLI are the one-dimensional nature of MLI, which neglects water-column dynamics beneath the ice and the simplified prediction of water surface temperature as a function of solar radiation reaching the water in MLI.

A comparison between observations and simulation results of the vertical profile of temperature, at the deepest part of the lake, is shown in Fig. 12; in general, the comparisons are excellent. The reverse winter stratification is well-modeled, with colder water overlying warmer water approaching 4°C near the lake bed. The surface waters warmed up a little later in the model in spring than the observations suggest, but for the remainder of the simulation period the comparisons are excellent. Convective mixing events, associated with warming of the water column, acting to homogenize the water column and deepen the stratification from 15 m to 22 m (Fig. 13), are simulated to occur with turbulent dissipation rates of 10^{-6}–10^{-7} m^2 s^{-3}. At other times, beneath the ice, dissipation remained negligible.

Discussion

The model results may be compared with data from other observational studies. The sharp temperature gradient immediately beneath the ice (Fig. 12) is characteristic of other small lakes (Bengtsson 1996; Forrest et al. 2008), as is the reverse stratification occurring beneath ice cover (Farmer and Carmak 1981). Similar observations do not exist for other Great Lakes. However, in the shallow nearshore ice-covered regions, of Lake Ontario, the modeled water-column dynamics are analogous to small lake systems (Fig. 8a).

The accuracy of the predictions for Lake Ontario may be compared to those reported by Wang et al. (2010) in their model application to Lake Erie. Both modeling efforts reasonably predict SST (present: MBD = −2.5% and

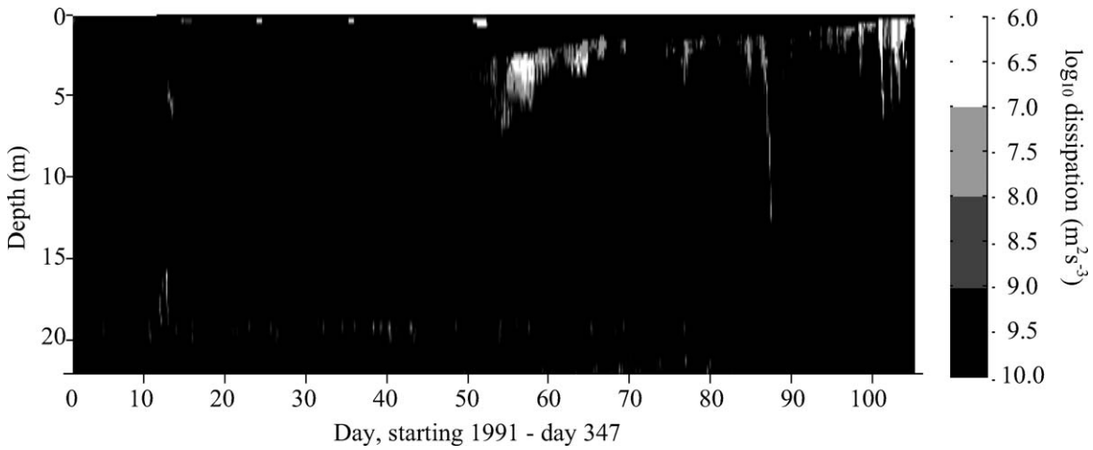

Fig. 13. Depth vs. time contours of modeled dissipation of turbulent kinetic energy ($\log_{10}$ dissipation) in Harmon Lake during 1991–1992. The lake is ice covered throughout the entire simulation.

RMSD = 1.0°C; Wang et al. [2010]: MBD = 1.5% and RMSD = 1.0°C). Ice-cover simulations (ice volume and surface area) are also similar (present model: MBD = −1.9% and RMSD = 1.4 cm; Wang et al. [2010]: MBD = 7.4% and RMSD = 1.84 cm), showing that including the process of ice advection does not lead to improvements in the overall prediction of ice-cover characteristics, although ice advection is likely important in the spatial patterns of ice coverage in large lakes during partial ice cover. The lack of observational data on ice thickness and low accuracy of the ice data extracted from satellite imagery makes further verification of the models difficult. The ice cover isolates the lake from the air; however, other mechanisms such as wind-induced oscillation of the ice cover can generate seiches and enhance mixing. Although very little observational data exist to quantify this process, the horizontal mixing coefficients could be in the other of 100 $cm^{-2}\,s^{-1}$ (Bengtsson 1996). Such mechanisms are neglected in this study. 8

In the winter season, physical observations of lake hydrodynamics under ice cover are difficult (Forrest et al. 2008) and infrequent (Mortimer and Mackereth 1958; Farmer and Carmack 1981). Using ELCOM with the ice-formation capability, we can better investigate winter lake processes that ultimately influence biogeochemistry, such as thermal bar and inverse winter stratification. Studies on fundamental limnology and source-water management, in cold climates, may be more easily extended through the winter, and ELCOM can be used for multiyear climate-change–coupled atmosphere–lake modeling (Leon et al. 2007).

A three-component ice-formation algorithm for blue ice, with ice and snow, has been added to ELCOM, extending the capability of the model for full-year simulations in regions that experience seasonal ice cover. Unlike previous lake-ice applications, the model allowed for significant variation of parameters (e.g., albedo, snow density) over short timescales, as is expected in mid-latitudes, and coupling to a three-dimensional hydrodynamic lake model provided the temporal and spatial variability needed to simulate lake biogeochemistry. The model was validated against observed data from both small and large Canadian lakes located in mid-latitude modeled temperatures; the percentage of lake surface covered with ice and the ice thickness were typically within 1°C, 5%, and 2 cm of observations, respectively. The evolution of the thermal structure from reverse winter stratification through spring turnover was also correctly simulated. The model was highly sensitive to the snow and ice parameters; further research on quantitative physical observation of ice cover is essential for improved numerical simulation.

Acknowledgments

Daniel Botelho performed the initial implementation of the Rogers et al. (1995) ice model into Estuary and Lake Computer Model (ELCOM). We acknowledge funding from the Environment Canada Lake Simcoe Cleanup Fund, Queen's University, and the Western Australian Water Corporation. The Lake Ontario temperature profile data and the Burlington meteorological data was provided by Ram Yerubandi at the National Water Research Institute, Environment Canada. The Lake Ontario precipitation data was provided by Tim Hunter at National Oceanic and Atmospheric Administration and the Sea Surface Temperature data by George Leshkevich at National Oceanic and Atmospheric Administration, Great Lakes Environmental Research Laboratory. We also would like to thank the reviewers of this manuscript for their insight and suggestions. This paper forms Center for Water Research reference 2384.

References

Ashton, G. D. [ed.]. 1986. River and lake ice engineering. Water Resources.

Bengtsson, L. 1996. Mixing in ice-covered lakes. Hydrobiologia **322:** 91–97, doi:10.1007/BF00031811

Boegman, L., and R. Yerubandi Rao. 2010. Process oriented modeling of Lake Ontario hydrodynamics, p. 1–6. *In* G. C. Christodoulou and A. I. Stamou [eds.], Proceedings 6th International Symposium on Environmental Hydraulics. 9

Botelho, D., and J. Imberger. 2007. Down-scaling model resolution to illuminate the internal wave field in a small stratified lake. J. Hydraul. Eng.-ASCE **133:** 1206–1218, doi:10.1061/(ASCE)0733-9429(2007)133:11(1206)

———, ———, C. Dallimore, and B. R. Hodges. 2009. A hydrostatic/non-hydrostatic grid-switching strategy for computing high-frequency, high wave number motions embedded in geophysical flows. Environ. Modell. Softw. **24:** 473–488, doi:10.1016/j.envsoft.2008.09.008

Birge, E. A., C. Juday, and H. W. March. 1927. The temperature of the bottom deposits of Lake Mendota; a chapter in the heat exchanges of the lake. Trans. Wis. Acad. Sci. **23:** 187–231.

Boer, K. W. 1980. The terrestrial solar spectrum, p. 65–87. *In* W. C. Dickinson and P. N. Chercmisinoff [eds.], Solar energy technology handbook, part A. Dekker.

Chapra, S. C. [ed.]. 1986. Surface water-quality modeling. WCB/McGraw-Hill.

Farmer, D. M. 1975. Potential temperatures in deep freshwater lakes. Limnol. Oceanogr. **20:** 634–635, doi:10.4319/lo.1975.20.4.0634

———, and E. Carmack. 1981. Wind mixing and re-stratification in a lake near the temperature of maximum density. J. Phys. Oceanogr. **11:** 1516–1533, doi:10.1175/1520-0485(1981)011<1516:WMARIA>2.0.CO;2

Forrest, A. L., B. E. Laval, R. Peters, and D. S. S. Lim. 2008. Convectively driven transport in temperate lakes. Limnol. Oceanogr. **53:** 2321–2332, doi:10.4319/lo.2008.53.5_part_2.2321

Gilpin, R. R., T. Hirata, and K. C. Cheng. 1980. Wave formation and heat transfer at an ice-water interface in the presence of a turbulent flow. J. Fluid Mech. **99:** 619–640, doi:10.1017/S0022112080000791

Gosink, J. P. 1987. Northern lake and reservoir modeling. Cold Regions Science and Technology **13:** 281–300, doi:10.1016/0165-232X(87)90008-5

Gottlieb, L. 1980. Development and applications of a runoff model for snow covered and glacierized basins. Nord. Hydrol. **11:** 255–272.

Hall, E. 2008. Hydrodynamic modeling of Lake Ontario. M. Eng. thesis. Queen's Univ.

Hamilton, D. P., C. M. Spillman, K. L. Prescott, T. K. Kratz, and J. J. Magnuson. 2002. Effects of atmospheric nutrient inputs and climate change on the trophic status of Crystal Lake, Wisconsin. Verh. Int. Verein. Limnol. **28:** 467–470.

Henderson-Sellers, B. 1984. Engineering limnology. Pitman.

———. 1986. Calculating the surface energy balance for lake and reservoir modeling: A review. Rev. Geophys. **24:** 625–649, doi:10.1029/RG024i003p00625 10

Hibler, W. D. 1980. Modeling a variable thickness sea ice cover. Mon. Weather Rev. **108:** 1943–1973, doi:10.1175/1520-0493(1980)108<1943:MAVTSI>2.0.CO;2

Hill, J. M., and A. Kucera. 1983. Freezing a saturated liquid inside a sphere. Int. J. Heat Mass Tran. **26:** 1631–1638, doi:10.1016/S0017-9310(83)80083-0

Hillmer, I. A., P. van Reenen, J. Imberger, and T. Zohary. 2008. Phytoplankton patchiness and their role in the modeled productivity of a large, seasonally stratified lake. Ecol. Model. **218:** 49–59, doi:10.1016/j.ecolmodel.2008.06.017

Hodges, B. R. 2009. Hydrodynamical modeling, p. 613–627. *In* G. E. Likens [ed.], Encyclopedia of inland waters. Elsevier.

———, and C. Dallimore. 2006. Estuary, lake and coastal ocean model: ELCOM science manual report. Perth, Western Australia: Centre for Water Research, University of Western, Australia; [accessed year month day]. Available from www.cwr.uwa.edu.au/…/models/elcom2/…/elcom_science…/ELCOM_Science.pdf.

———, J. Imberger, A. Saggio, and K. B. Winters. 2000. Modeling basin-scale internal waves in a stratified lake, J. Limnol. Oceanogr. **45:** 1603–1620.

Ikeda, M., T. Yao, and Q. Yao. 1996. Seasonal evolution of sea ice cover and shelf water off Labrador simulated in a coupled ice–ocean model. J. Geophys. Res. **101:** 465–489, doi:10.1029/96JC00716

Kirk, J. T. O. 1983. Light and photosynthesis in aquatic ecosystems. Cambridge Press.

Koren, V., J. Schaake, K. Mitchell, Q. Y. Duan, F. Chen, and J. M. Baker. 1999. A parameterization of snowpack and frozen ground intended for NCEP weather and climate models. J. Geophys. Res. **104:** 19569–19585, doi:10.1029/1999JD900232

Leon, L. F., D. C.-L. Lam, W. M. Schertzer, D. Swayne, and J. Imberger. 2007. Towards coupling a 3D hydrodynamic lake model with the Canadian Regional Climate Model: Simulation on Great Slave Lake. Environ. Modell. Softw. **22:** 787–796, doi:10.1016/j.envsoft.2006.03.005

Likens, G. E., and N. M. Johnson. 1969. Measurement and analysis of the annual heat budget for the sediments in two Wisconsin lakes. Limnol. Oceanogr. **14:** 115–135, doi:10.4319/lo.1969.14.1.0115

Maykut, G. A., and N. Untersteiner. 1971. Some results from a time-dependent Thermodynamic model of sea ice. J. Geophys. Res. **76:** 1550–1575, doi:10.1029/JC076i006p01550

McCord, S. A., S. G. Schladow, and T. G. Miller. 2000. Modeling artificial aeration kinetics in ice covered lakes. J. Environ. Eng.-ASCE. **126:** 21–31, doi:10.1061/(ASCE)0733-9372(2000)126:1(21)

Morillo, S., J. Imberger, J. P. Antenucci, and D. Copetti. 2009. Using impellers to distribute local nutrient loadings in a stratified lake; Lake Como, Italy. J. Hydraul. Eng.-ASCE **135:** 564–574, doi:10.1061/(ASCE)HY.1943-7900.0000048

Mortimer, C. H., and F. J. H. Mackereth. 1958. Convection and its consequences in ice-covered lakes. Verh. Int. Verein. Theor. Angew. Limnol. **13:** 923–932.

Nghiem, S. V., and G. A. Leshkevich. 2007. Satellite SAR remote sensing of Great Lakes ice cover. Part 1. Ice backscatter signatures at C band. J. Great Lakes Res. **33:** 722–735, doi:10.3394/0380-1330(2007)33[722:SSRSOG]2.0.CO;2

Parkinson, C., and W. Washington. 1979. A large-scale numerical model of sea ice. J. Geophys. Res. **84:** 311–337, doi:10.1029/JC084iC01p00311

Patterson, J. C., and P. F. Hamblin. 1988. Thermal simulation of a lake with winter ice cover. Limnol. Oceanogr. **33:** 323–338, doi:10.4319/lo.1988.33.3.0323

Rogers, C. K. 1992. Impact of an artificial circulation device on the heat budget of an ice-covered mid-latitude lake. M.S. thesis, Univ. British Columbia.

———, G. Lawrence, and P. F. Hamblin. 1995. Observations and numerical simulation of a shallow ice-covered mid-latitude lake. Limnol. Oceanogr. **40:** 374–385, doi:10.4319/lo.1995.40.2.0374

Rumer, R. R., A. Wake, and S. H. Shieh. 1981. Development of an ice dynamics forecasting model for Lake Erie research report No. 81-1. Buffalo (NY): Department of Civil Engineering, Center for Cold Regions Science and Technology, State University of New York at Buffalo.

Semtner, A. J. 1976. A model for thermodynamic growth of sea ice in numerical investigations of climate. J. Phys. Oceanogr. **6:** 379–389, doi:10.1175/1520-0485(1976)006<0379:AMFTTG>2.0.CO;2

Shore, J. 2009. Modeling the circulation and exchange of Kingston Basin and Lake Ontario with FVCOM. Ocean Modell. **30:** 106–114, doi:10.1016/j.ocemod.2009.06.007

Vavrus, S. J., R. H. Wynne, and J. A. Foley. 1996. Measuring the sensitivity of southern Wisconsin lake ice to climate variations and lake depth using a numerical model. Limnol. Oceanogr. **41:** 822–831, doi:10.4319/lo.1996.41.5.0822

Wake, A., and R. R. Rumer. 1979. Modeling the ice regime of Lake Erie. J. Hydraul. Eng.-ASCE **105:** 827–844.

Wang, J., H. Hu, D. Schwab, D. Beletsky, A. Clites, and G. Leshkevich. 2010. Development of the Great Lakes ice-circulation model (GLIM): Application to Lake Erie in 2003–2004. J. Great Lake Res. **36:** 425–436, doi:10.1016/j.jglr.2010.04.002

Welch, H. E., and M. Bergmann. 1985. Water circulation in small arctic lakes in winter. Can. J. Fish. Aquat. Sci. **42:** 506–520, doi:10.1139/f85-068

Yao, T., C. L. Tang, and I. K. Peterson. 2000. Modeling the seasonal variation of sea ice in the Labrador Sea with a coupled multicategory ice model and the Princeton ocean model. J. Geophys. Res. **105:** 1153–1165, doi:10.1029/1999JC900264

Associate editor: Chris Rehmann

Received: 12 January 2011
Accepted: 24 August 2011
Amended: 15 September 2011